ACS APPLIED MATERIALS & INTERFACES

RESEARCH ARTICLE

www.acsami.org

Effect of Highly Ordered Single-Crystalline TiO_2 Nanowire Length on the Photovoltaic Performance of Dye-Sensitized Solar Cells

Zheng-ji Zhou, Jun-qi Fan, Xia Wang, Wen-hui Zhou, Zu-liang Du, and Si-xin Wu*

Key Lab for Special Functional Materials of Ministry of Education, Henan University, Kaifeng 475004, China

Supporting Information

ABSTRACT: One-dimensional semiconductor nanostructures grown directly onto transparent conducting oxide substrates with a high internal surface area are most desirable for high-efficiency dye-sensitized solar cells (DSSCs). Herein, we present a multicycle hydrothermal synthesis process to produce vertically aligned, single crystal rutile TiO_2 nanowires with different lengths between 1 and 8 μm for application as the working electrode in DSSCs. Optimum performance was obtained with a TiO_2 nanowire length of 2.0 μm, which may be ascribed to a smaller nanowire diameter with a high internal surface area and better optical transmittance with an increase in the incident light intensity on the N719 dye; as well as a firm connection at the FTO/TiO_2 nanowire interface.

KEYWORDS: TiO_2 nanowire array, dye-sensitized solar cell, nanowire length, conversion efficiency

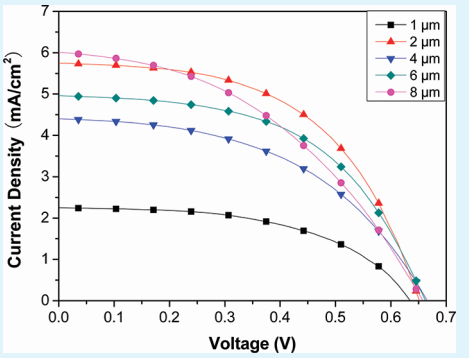

INTRODUCTION

Dye-sensitized solar cells (DSSCs) have been recognized as an attractive alternative to conventional solid-state homo- and heterojunction solar cells because of their reasonable solar-to-electricity conversion efficiency, low-cost materials, and simple fabrication on rigid and flexible substrates.[1−6] Traditional DSSCs use high-surface-area titania nanocrystalline thin films as the photosensitized anode material and a power conversion efficiency of 11.18% has been achieved.[7] However, a further increase in the conversion efficiency is impeded by slow electron percolation and recombination loss resulting from electron trap states that reside on the surface of the disordered nanoparticle network.[8−11] Many methods have been developed to facilitate the transmission of electrons to minimize recombination, such as the incorporation of hole-blocking layers,[12] the plasma-modification of mesoporous TiO_2 films[13,14] and the use of hierarchical semiconductor nanoarchitectures.[15−18] Among the nanoarchitectures used as photoanodes, an array of highly ordered, vertically aligned one-dimensional (1D) nanostructures, such as nanowires[19,20] and nanotubes,[21,22] offering direct electrical pathways for photogenerated electrons, have attracted extensive attention as a substitute for randomly oriented titania nanoparticles.[2,19−23]

So far, many efforts have been made to fabricate DSSCs using vertically aligned 1D nanostructures. However, despite the advantages of enhanced electron mobility, the energy conversion efficiency of DSSCs based on vertically aligned 1D nanostructure arrays as photoanodes is relatively lower than that of those prepared using conventional TiO_2 random polycrystalline nanoparticle networks. The main reason was attributed to the low internal surface area of 1D nanostructures, which result in deficient dye loading and light harvesting.[24−27] Normally, it is conjectured that fabrication of 1D vertically aligned nanostructure arrays with increased length scale could enlarge the internal surface area within the photoanode, thereby obtaining a higher efficiency.[2,19,27]

In this article, we report the preparation of highly ordered, single-crystalline rutile TiO_2 nanowire arrays with variable length on FTO substrates by multiple growth cycles, using a simple hydrothermal method. By investigating the relationship between the efficiency of different length of TiO_2 nanowire photoanodes and the approach for nanowire arrays formation, we have found that not only the internal surface area, but also the photon loss in traversing the nanowire photoelectrodes and the contact at the FTO−nanowire interface have a great effect on the photovoltaic performance of nanowire-based DSSCs.

EXPERIMENTAL SECTION

Synthesis of TiO_2 Nanowire Array Films with Different Lengths. Titanium butoxide was purchased from Sigma-Aldrich (China) and concentrated hydrochloric acid (36.5−38% by weight) was purchased from Tianjin Chemical Reagents Co.. All reagents were used without further purification. Triply deionized water (resistivity of 18.2 MΩ cm^{-1}) was obtained from a Milli-Q ultrapure water system (Millipore, USA). FTO-coated glass slides (F: SnO_2, 14 Ω/square, Nippon Sheet Glass Group, Japan) were thoroughly washed with a mixed solution of deionized water, acetone, and 2-propanol (volume ratios of 1:1:1) under sonication for 60 min.

TiO_2 nanowire array films were prepared by a hydrothermal method and the details of the synthetic procedure for the fabrication

Received: July 29, 2011
Accepted: October 3, 2011
Published: October 03, 2011

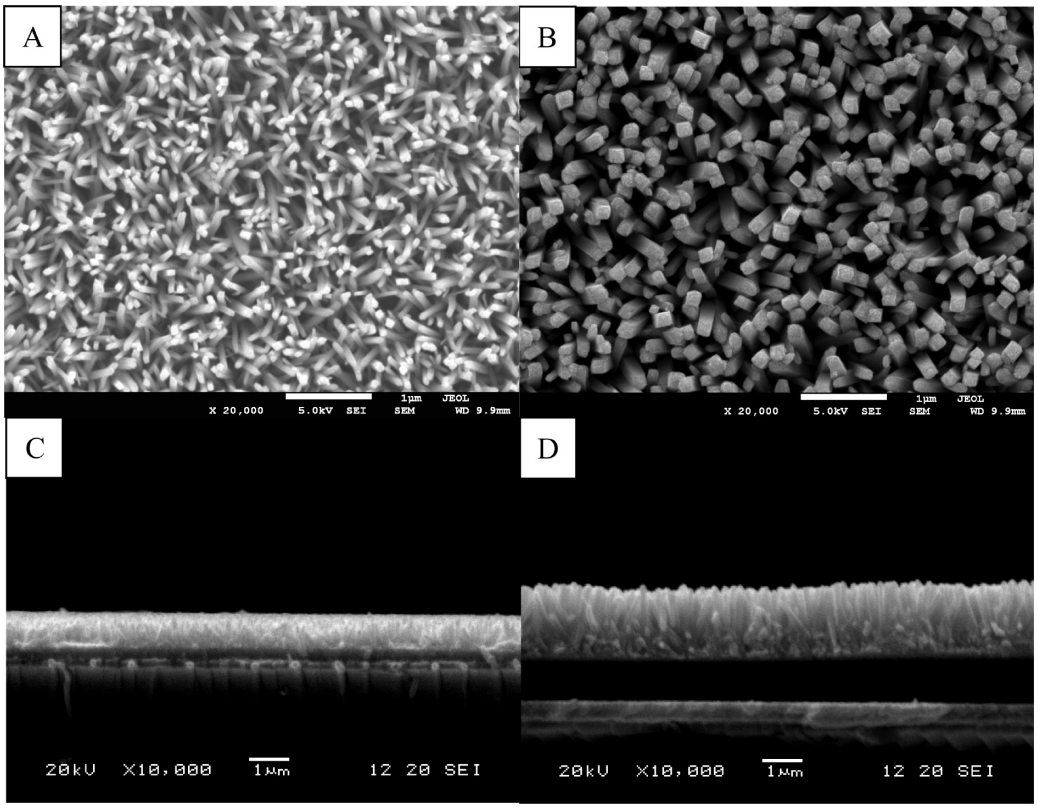

Figure 1. FESEM images of vertically aligned rutile TiO_2 nanowire array grown on FTO substrate at 150 °C for (A) 5 and (B) 10 h; (C, D) corresponding cross-sectional SEM images.

of TiO_2 nanowire arrays were similar to that described by Liu and Aydil.[20] Briefly, 30 mL of deionized water was mixed with 30 mL of concentrated hydrochloric acid in a Teflon-lined stainless steel autoclave (100 mL volume, Zhengzhou Hezhong Instrument Ltd. China). The mixture was stirred under ambient conditions for 5 min, and then 1 mL of titanium butoxide was added to the mixture followed by stirring for another 5 min. One piece of FTO substrate was placed at an angle against the wall of the reactor in the 100 mL Teflon liner, and the conductive side of FTO was placed face down. The hydrothermal synthesis was conducted at 150 °C for different growth times (5−20 h) in an electric oven. After synthesis, the autoclave was cooled to room temperature under flowing water and the FTO substrate was taken out, rinsed extensively with distilled water and dried in ambient air. To grow longer TiO_2 nanowire arrays, a multistep hydrothermal growth process was employed as follows: First, a TiO_2 nanowire array was grown on FTO substrate at 150 °C for 20 h. Second, we placed the FTO substrate obtained from the first step within another reactor filled with freshly prepared growth solution similarly to the previous one except for the addition of 5 mL of saturated aqueous NaCl, and the growth was conducted in this solution at 150 °C for another 20 h. This process may be repeated multiple times to obtain a desired length of TiO_2 nanowire array (see the Supporting Information, Figure SI-1).

Solar Cell Fabrication. The DSSCs were assembled as follows: The as-synthesized TiO_2 nanowire array films grown on FTO-covered glass were immersed overnight in a 0.3 mM ethanolic solution of *cis*-bis(isothiocyanato)bis(2,2′-bipyrridyl-4−4′-dicarboxylato)-ruthenium-(II)bis-tetrabutylammonium dye (N-719 as received from Solaronix) at room temperature to absorb the dye. The samples were then taken out and rinsed with ethanol to remove excess dye adsorbed and dried in air at room temperature. The counter Pt electrodes were prepared by sputtering with 100 nm of Pt on cleaned FTO glass using radio frequency sputtering at a power of 150 W and a working pressure of 3×10^{-3} Torr with argon gas for 60 s. The sandwich-type solar cell was assembled by placing a platinum-coated counter electrode on the N719 dye-sensitized photoelectrode (working electrode), and clipped together as an open cell for measurements. The cell was then filled with a liquid electrolyte composed of 0.1 M anhydrous LiI, 0.12 M I_2, 1.0 M 1,2-dimethyl-3-n-propylimidazolium iodide (DMPII), and 0.5 M tert-butylpyridine in dehydrated acetonitrile by capillary force.

Morphology, Structural Characterization, and Photoelectrochemical Measurements. The morphology of the as-prepared sample was studied by field-emission gun scanning electron microscopy (FESEM, JSM-7001F) and transmission electron microscopy (TEM/HRTEM, JEOL JEM-2100). The TiO_2 nanowires for TEM imaging were detached from the FTO substrate, followed by dispersion in ethanol by sonication. A few drops of the sonicated suspension were dropped onto a carbon film supported copper grid. The crystal structure was determined by X-ray diffraction (XRD). The XRD patterns were recorded using a Philips X'Pert PRO X-ray diffractometer with Cu Kα1 radiation (λ = 1.5406 Å) from 20 to 70° at a scan rate of 2.4° min^{-1}. X-ray tube voltage and current were set at 40 kV and 40 mA, respectively. The optical properties were examined by UV−visible spectroscopy (CARY5000 UV visible-NIR spectrometer). Photocurrent density−voltage ($J-V$) characteristics measurements were recorded using a digital source meter (Keithley 2400, computer-controlled) with the device under AM 1.5 G spectrum, which was produced by a solar simulator (Newport, Oriel class A, SP91160A, USA). The light power density was calibrated against a Si-based reference cell (Hamamatsu S1133) to accurately simulate the full-sun intensity (100 mW cm^{-2}).

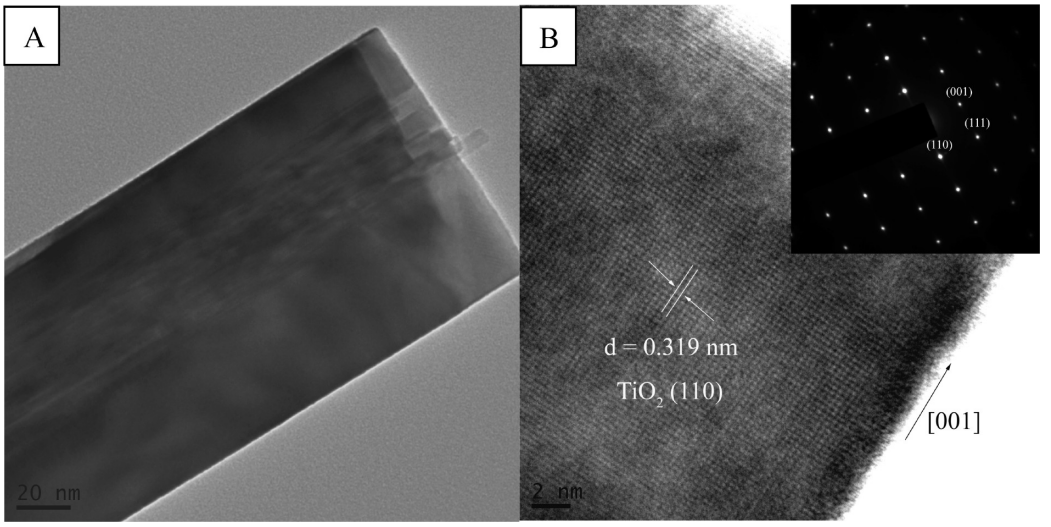

Figure 2. TEM image of a (A) single TiO_2 nanowire, (B) HRTEM image of the same nanowire. The inset shows the selected-area electron diffraction pattern.

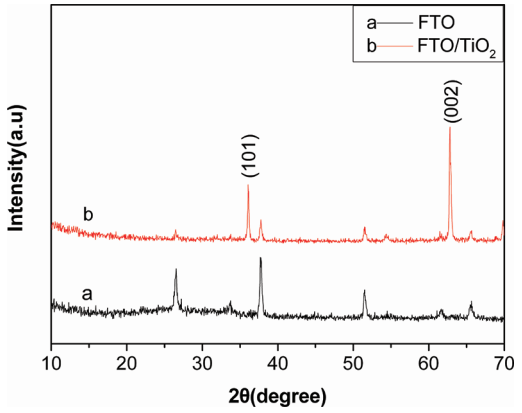

Figure 3. X-ray diffraction pattern of vertically oriented TiO_2 nanowires on FTO coated glass.

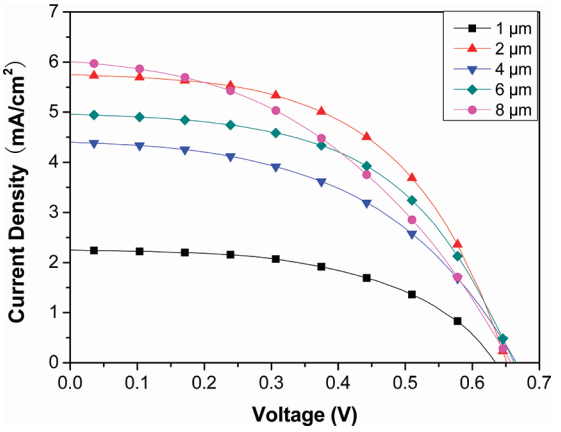

Figure 4. Photocurrent−photovoltage characteristics of DSSCs assembled with different TiO_2 nanowire lengths. The curves were measured under stimulated AM 1.5 G sunlight illumination with a light intensity of 100 mW cm^{-2}.

RESULTS AND DISCUSSION

Characterization of the TiO_2 Nanowire Array. Images A and B in Figure 1 are field-emission scanning electron microscope images of the nanowire array films grown at 150 °C for 5 and 10 h, respectively. These images clearly indicate that the entire surface of the FTO substrate is covered uniformly and densely with vertically oriented TiO_2 nanowires, and the nanowires are tetragonal in shape with square top facets, which is the typical growth habit for the tetragonal crystal structure. Moreover, it is obvious that the diameter of the nanowires increased upon prolonging the reaction time, and many step edges are present at the top surface of the nanowires, which can serve as nucleation sites for the further growth of nanowires by the addition of titanium growth units. From the cross-sectional view of the samples, we can see that the nanowires grow almost perpendicularly from the substrate. Furthermore, the length of the TiO_2 nanowire array films can be easily controlled by adjusting the growth duration and the hydrothermal treatment cycles (see the Supporting Information, Figure SI-2).

A detailed microscopic characterization of the TiO_2 nanowires was carried out using transmission electron microscopy (TEM), high-resolution TEM (HRTEM), and selected area electron diffraction (SAED). Figure 2A shows the TEM image of a single TiO_2 nanowire. The SAED pattern of the same TiO_2 nanowire is shown in the inset of Figure 2B. The well-aligned spots indicate that the nanowires are single crystals, which was further confirmed by the HRTEM image (Figure 2B). A lattice spacing of 0.319 nm between the adjacent lattice fringes is distinctly visible and can be assigned to the interplanar distance of tetragonal rutile TiO_2 (110). The nanowires grow along the (110) crystal plane with a preferred (001) orientation.

Figure 3 shows the X-ray diffraction (XRD) pattern of the FTO substrate before and after the hydrothermal growth of TiO_2 nanowires. Compared with curve a, additional peaks appear in curve b, which can be indexed to the tetragonal rutile phase of TiO_2 (JCPDS file no. 88−1175); a significantly enhanced (002) peak at a 2-theta of 63.20 indicates that the nanowires are well crystallized throughout their length and grow preferentially along the [001] direction with the growth axis perpendicular to

Table 1. Photovoltaic Performance of DSSCs Fabricated with Various Length of TiO_2 Nanowire Arrays

length of nanowires (μm)	J_{sc} (mA/cm^2)	V_{oc} (V)	fill factor (%)	efficiency (η%)
1.0	2.273 ± 0.016	0.633 ± 0.004	52.389 ± 0.136	0.754 ± 0.003
2.0	5.745 ± 0.026	0.652 ± 0.001	53.135 ± 0.498	1.991 ± 0.010
4.0	4.395 ± 0.010	0.666 ± 0.001	48.546 ± 0.144	1.421 ± 0.003
6.0	4.971 ± 0.048	0.660 ± 0.004	53.436 ± 0.276	1.754 ± 0.002
8.0	5.994 ± 0.116	0.658 ± 0.002	43.053 ± 0.703	1.698 ± 0.003

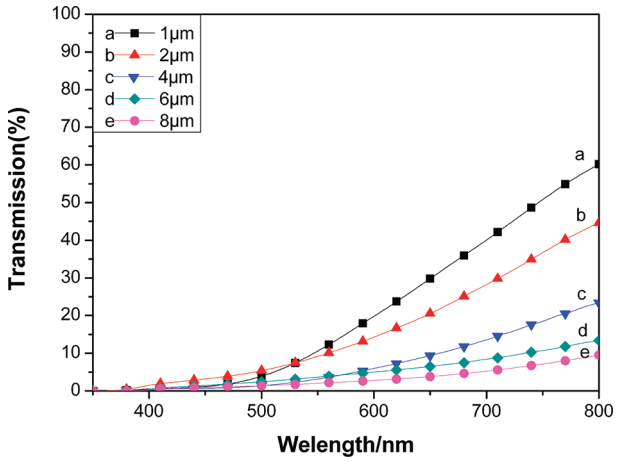

Figure 5. Optical transmittance spectra of TiO_2 nanowire array films with a nanowire length of (a) 1.0, (b) 2.0, (c) 4.0, (d) 6.0, and (e) 8.0 μm.

the substrate, which agrees well with the HRTEM and SAED measurements.

Effect of TiO_2 Nanowire Length on the Photovoltaic Performance of DSSCs. In recent studies, the electron diffusion length of 1D nanostructure arrays have been estimated to be 100 μm,[28−30] and it is generally believed that the internal surface area and the amount of dye adsorbed increases as a function of the 1D nanowire length. From these points of view, with an increase in the nanowire length the performance of DSSCs should be improved. In our contrast experiments where the same batch of N-719 dye was used with a similar redox electrolyte and equivalent active areas, the current−voltage characteristic of the solar cells assembled using different lengths of TiO_2 nanowire arrays are shown in Figure 4. The statistical performance is shown in Table 1, from which we can see the DSSC assembled with about 2.0 μm TiO_2 nanowire array by hydrothermal growth of 10 h has a short-circuit current (J_{sc}) of 5.8 mA/cm^2 and an open-circuit voltage (V_{oc}) of 0.65 V, which exhibits the best performance with an overall power conversion efficiency (η) of 1.99% and a fill factor (FF) of 0.53. The performance of the solar cells does not constantly improve with a further increase in the length of the TiO_2 nanowires and the efficiency initially decreased to 1.42% for the 4.0 μm nanowires and then increased to 1.75% for the 6.0 μm nanowires, whereafter it decreased again to 1.70% when the length of TiO_2 nanowires was about 8.0 μm.

The variation in solar cell performance has to do with the context of nanowire array formation and can be explained by the following three factors: First of all, longer nanowire arrays of 4.0 μm were obtained by extending the reaction time, during this process, the length and diameter of the nanowires grew simultaneously. In fact, by increasing the duration of hydrothermal growth, the TiO_2 nanowires fused at their roots to form a continuous film due to an increase in the lateral dimension.[5,19,20] The widening and fusion of nanowires decreased the packing density per unit area of the nanowire arrays, and therefore, a significant percentage of the surface area gained by increasing the wire length is lost, as small changes in the width of the nanowires can have a large effect on the surface area of the nanowire arrays. The diameter of TiO_2 nanowires increased from 60 to 100 nm when the reaction time was extended from 10 to 20 h. Despite the fact that the nanowires grew taller, the effective internal surface area actually decreased, resulting in the decline in efficiency. However, the efficiency increased again when the length of the TiO_2 nanowires increased from 4.0 to 6.0 μm after a two-step hydrothermal growth process, which is due to the addition of a saturated NaCl aqueous solution in the second growth period. Cl^- can preferentially adsorb on to the (110) crystal plane of TiO_2, and thus the growth rate of the (110) face, in other words, the lateral growth speed is retarded.[31−33] Therefore, after the second growth cycle the nanowires grew taller but the diameter remained constant, which resulted in an increase in the surface area. This can be further verified by measuring the absorbance of dye desorbed from the TiO_2 photoelectrodes using a mixed solution of 0.1 M NaOH and ethanol (1:1 in volume fraction) by UV−vis spectroscopy (see the Supporting Information, Figure SI-3).

The second factor may be ascribed to the lower light transmittance of TiO_2 nanowire array films with an increase in nanowire length. As shown in Figure 5, a linear decrease in transmittance is evident when the length of the TiO_2 nanowires increased from 1.0 to 8.0 μm, which would reduce the incident light intensity on the dye adsorbed onto the top surface of TiO_2 and result in a lower increase in the injection current from the excited dyes to the conduction band of TiO_2.[34,35] Thus, for longer TiO_2 nanowires the top of the nanowire array does not contribute significantly to an improvement in the photovoltaic performance. The third factor is that the contact between the nanowire and FTO becomes weaker with an extension of the reaction time. We have noticed that the nanowire arrays easily peel off the FTO substrate after multiple growth cycles. The weaker interface degrades the photoelectrochemical properties of the devices.[19] Because of the lower transmittance and weaker interfaces after the third growth cycle the performance decreases again, despite the increase in nanowire length.

It is noteworthy that the efficiency of the nanowire cell is still much lower than the current state of the TiO_2 nanoparticle based DSSC. In our experiment, the highest efficiency was carried out on the rutile TiO_2 array with nanowire diameters of about 60 nm and lengths about 2.0 μm. For mesoporous TiO_2 films that was composed of anatase phase of TiO_2 nanocrystals, the photoelectrodes used for DSSCs have a typical TiO_2 nanoparticles diameter of less than 30 nm, and the thickness of the TiO_2 films

is more than 8 μm. It is obvious that the insufficient surface area of the 1D nanowire arrays result in poor dye loadings and light harvesting. Besides, the rutile phase of TiO_2 nanowires, compared with anatase which is the most appropriate phase of titania for use in DSCCs, is lower activity.[36,37] All these matter constrains the energy conversion efficiency of the TiO_2 nanowire cell to relatively low levels. Potential ways of fully employing the superior charge transport property of 1D TiO_2 nanowire arrays and increasing the power conversion efficiency of nanowire-based dye-sensitized solar cells include designing anatase nanowire array films with smaller diameters and higher packing densities, as well as ensuring an improved electrical contact with the transparent conducting substrate to reduce the charge loss in transmission.

CONCLUSION

In summary, different lengths of single-crystal TiO_2 nanowire arrays were successfully prepared on FTO-coated glass substrates by a facile multicycle hydrothermal method. The influence of TiO_2 nanowire length on the photovoltaic performance of the dye sensitized solar cells was investigated. The best photovoltaic performance with an efficiency of 2.0% was obtained for a 2.0 μm long nanowire array. A further increase in the length of the TiO_2 nanowires did not result in the expected increase in photoconversion efficiency. This can be explained by decrease in the internal surface area because of widening and fusion at the base of the nanowires, the diminishing incident light intensity due to filter in traversing the longer TiO_2 nanowires and the weakening interface between nanowire and FTO. We believe that the results herein will be of significant use for design of novel and superior nanoarchitecture photoanodes for DSSCs.

ASSOCIATED CONTENT

Supporting Information. Detailed experimental setup and schematic process for growing longer TiO_2 nanowire arrays on FTO, SEM images of cross-sectional view of vertically oriented TiO_2 nanowire films grown over different times and cycles, absorption spectra of dye desorbed from different lengths of TiO_2 nanowire array photoelectrodes, absorption spectra of the different lengths of TiO_2 nanowire array photoelectrodes sensitized by N719 dye and reflectance spectra of TiO_2 nanowire films with different nanowire length. This material is available free of charge via the Internet at http://pubs.acs.org.

AUTHOR INFORMATION

Corresponding Author
*E-mail: wusixin@henu.edu.cn.

ACKNOWLEDGMENT

This project is supported by the National Natural Science Foundation of China (20871041 and 20903033) and the New Century Excellent Talents in University (NCET-08-0659).

REFERENCES

(1) Grätzel, M. *Nature* **2001**, *414*, 338–344.
(2) Varghese, O. K.; Paulose, M.; Grimes, C. A. *Nat. Nanotechnol.* **2009**, *4*, 592–597.
(3) Hagfeldt, A.; Boschloo, G.; Sun, L.; Kloo, L.; Pettersson, H. *Chem. Rev.* **2010**, *110*, 6595–6663.
(4) Xu, F.; Dai, M.; Lu, Y.; Sun, L. *J. Phys. Chem. C* **2010**, *114*, 2776–2782.
(5) Xu, C. K.; Wu, J. M.; Desai, U. V.; Gao, D. *J. Am. Chem. Soc.* **2011**, *133*, 8122–8125.
(6) Hwang, D.; Jo, S. M.; Kim, D.; Y.; Armel, V.; MacFarlane, D. R.; Jang, S. Y. *ACS Appl. Mater. Interfaces* **2011**, *3*, 1521–1527.
(7) Nazeeruddin, M. K.; De Angelis, F.; Fantacci, S.; Selloni, A.; Viscardi, G.; Liska, P.; Ito, S.; Takeru, B.; Grätzel, M. *J. Am. Chem. Soc.* **2005**, *127*, 16835–16847.
(8) Fisher, A. C.; Peter, L. M.; Ponomarev, E. A.; Walker, A. B.; Wijayanta, K. G. U. *J. Phys. Chem. B* **2000**, *104*, 949–958.
(9) Law, M.; Greene, L. E.; Johnson, J. C.; Saykally, R.; Yang, P. D. *Nat. Mater.* **2005**, *4*, 455–459.
(10) Nissfolk, J.; Fredin, K.; Hagfeldt, A.; Boschloo, G. *J. Phys. Chem. B* **2006**, *110*, 17715–17718.
(11) Zhang, Y.; Xie, Z. B.; Wang, J. *ACS Appl. Mater. Interfaces* **2009**, *1*, 2789–2795.
(12) Mane, R. S.; Lee, W. J.; Pathan, H. M.; Han, S. H. *J. Phys. Chem. B* **2005**, *109*, 24254–24259.
(13) Pulsipher, D. J. V.; Fisher, E. R. *Surf. Coat. Technol.* **2009**, *203*, 2236–2242.
(14) Pulsipher, D. J. V.; Martin, I. T.; Fisher, E. R. *ACS Appl. Mater. Interfaces* **2010**, *2*, 1743–1753.
(15) Jiang, C. Y.; Sun, X. W.; Lo, G. Q.; Kwong, D. L. *Appl. Phys. Lett.* **2007**, *90*, 263501–263503.
(16) Xu, F.; Dai, M.; Lu, Y. N.; Sun, L. T. *J. Phys. Chem. C* **2010**, *114*, 2776–2782.
(17) Zhang, Q. F.; Cao, G. Z. J. *Mater. Chem.* **2011**, *21*, 6769–6774.
(18) Shao, F.; Sun, J.; Gao, L.; Yang, S. W.; Luo, J. Q. *ACS Appl. Mater. Interfaces* **2011**, *3*, 2148–2153.
(19) Feng, X.; Shankar, K.; Varghese, O. K.; Paulose, M.; Latempa, T. J.; Grimes, C. A. *Nano Lett.* **2008**, *8*, 3781–3786.
(20) Liu, B.; Aydil, E. S. *J. Am. Chem. Soc.* **2009**, *131*, 3985–3990.
(21) Jennings, J. R.; Ghicov, A.; Peter, L. M.; Schmuki, P.; Walker, A. B. *J. Am. Chem. Soc.* **2008**, *130*, 13364–13372.
(22) Kim, J. Y.; Noh, J. H.; Zhu, K.; Halverson, A. F.; Neale, N. R.; Park, S.; Hong, K. S.; Frank, A. J. *ACS Nano* **2011**, *5*, 2647–2656.
(23) Hwang, D.; Jo, S. M.; Kim, D. Y.; Armel, V.; MacFarlane, D. R.; Jang, S. Y. *ACS Appl. Mater. Interfaces* **2011**, *3*, 1521–1527.
(24) Mor, G. K.; Shankar, K.; Paulose, M.; Varghese, O. K.; Grimes, C. A. *Nano Lett.* **2006**, *6*, 215–218.
(25) Xu, C.; Shin, P.; Cao, L.; Wu, J.; Gao, D. *Chem. Mater.* **2010**, *22*, 143–148.
(26) Ko, S. H.; Lee, D.; Kang, H. W.; Nam, K. H.; Yeo, J. Y.; Hong, S. J.; Grigoropoulos, C. P.; Sung, H. J. *Nano Lett.* **2011**, *11*, 666–671.
(27) Xu, C. K.; Wu, J. M.; Desai, U. V.; Gao, D. *J. Am. Chem. Soc.* **2011**, *133*, 8122–8125.
(28) Galoppini, E.; Rochford, J.; Chen, H.; Saraf, G.; Lu, Y.; Hagfeldt, A.; Boschloo, G. *J. Phys. Chem. B* **2006**, *110*, 16159–16161.
(29) Martinson, A. B. F.; Goes, M. S.; Fabregat-Santiago, F.; Bisquert, J.; Pellin, M. J.; Hupp, J. T. *J. Phys. Chem. A* **2009**, *113*, 4015–4021.
(30) Jennings, J. R.; Ghicov, A.; Peter, L. M.; Schmuki, P.; Walker, A. B. *J. Am. Chem. Soc.* **2008**, *130*, 13364–13372.
(31) Hosono, E.; Fujihara, S.; Kakiuchi, K.; Imai, H. *J. Am. Chem. Soc.* **2004**, *126*, 7790–7791.
(32) Kakiuchi, K.; Hosono, E.; Imai, H.; Kimura, T.; Fujihara, S. J. *Cryst. Growth* **2006**, *293*, 541–545.
(33) Feng, X. J.; Zhai, J.; Jiang, L. *Angew. Chem., Int. Ed.* **2005**, *44*, 5115–5118.
(34) Ito, S.; Zakeeruddin, S. M.; Humphry-Baker, R.; Liska, P.; Charvet, R.; Comte, P.; Nazeeruddin, M. K.; Pechy, P.; Takata, M.; Miura, H.; Uchida, S.; Grätzel, M. *Adv. Mater.* **2006**, *18*, 1202–1205.
(35) Kao, M. C.; Chen, H. Z.; Young, S. L.; Kung, C. Y.; Lin, C. C. *Thin Solid Films* **2009**, *517*, 5096–5099.
(36) Hagfeldt, A.; Grätzel, M. *Chem. Rev.* **1995**, *95*, 49–68.
(37) Kavan, L.; Grätzel, M.; Gilbert, S. E.; Klemenz, C.; Scheel, H. J. *J. Am. Chem. Soc.* **1996**, *118*, 6716–6723.